Acta Biomaterialia 79 (2018) 354–363

Contents lists available at ScienceDirect

Acta Biomaterialia

journal homepage: www.elsevier.com/locate/actabiomat

Full length article

Autophagic response to cellular exposure to titanium dioxide nanoparticles

Lauren Popp [a], Vinh Tran [b], Risha Patel [a], Laura Segatori [a,b,*]

[a] Rice University, Department of Chemical and Biomolecular Engineering, 6100 Main St, MS-362, Houston, TX 77005, USA
[b] Rice University, Department of BioSciences, 6100 Main St, MS-362, Houston, TX 77005, USA

ARTICLE INFO

Article history:
Received 21 March 2018
Received in revised form 30 July 2018
Accepted 17 August 2018
Available online 19 August 2018

Keywords:
Titanium dioxide
Nanoparticle
Autophagy
Lysosome
Transcription factor EB

ABSTRACT

Titanium dioxide is "generally regarded as safe" and titanium dioxide nanoparticles (TiO_2 NPs) are used in a wide variety of consumer products. Cellular exposure to TiO_2 NPs results in complex effects on cell physiology including induction of oxidative stress and impairment of lysosomal function, raising concerns about the impact of TiO_2 NPs on biological systems. We investigated the effects of TiO_2 NPs (15, 50, and 100 nm in diameter) on the lysosome-autophagy system, the main cellular catabolic pathway that mediates degradation of nanomaterials. Specifically, we monitored a comprehensive set of markers of the lysosome-autophagy system upon cell exposure to TiO_2 NPs, ranging from transcriptional activation of genes required for the formation of autophagic vesicles to clearance of autophagic substrates. This study reveals that uptake of TiO_2 NPs induces a response of the lysosome-autophagy system mediated by the transcription factor EB and consequent upregulation of the autophagic flux. Prolonged exposure to TiO_2 NPs, however, was found to induce lysosomal dysfunction and membrane permeabilization, leading to a blockage in autophagic flux. Results from this study will inform the design of TiO_2 NP based devices with specific autophagy-modulating properties.

1. Introduction

Recent progress in the field of nanotechnology has not only led to the design of multifunctional nanotherapeutics [1] and advanced nano-biosensors [2], but has also resulted in a rapid increase in the number of consumer products containing nanomaterials [3]. The commercialization of nanomaterial-based products has paralleled an increase in the large-scale production of nanomaterials and, thus, a growing concern regarding the potentially adverse effects of exposure of employees, consumers, and patients. It is widely accepted that engineered nanomaterials exert a diverse array of effects on human health, paralleling the heterogeneous and complex properties of the nano-sized materials themselves [4]. The health effects of nanomaterials, such as induction of the inflammatory response, neurodegeneration, or cancer, are ultimately a consequence of the interactions between nanomaterials and cellular components that also operate at the nanoscale.

Internalization of nanomaterials into cells activates the response of a series of cellular pathways precisely evolved to prevent accumulation of toxic or aberrant material and maintain cellular homeostasis. In particular, a variety of nano-sized materials encountered by the cell, including intracellular protein aggregates and damaged organelles, as well as internalized pathogens and anthropogenic nanomaterials, activate the response of the lysosome-autophagy system. As the main catabolic pathway in mammalian cells, macroautophagy (hereafter referred to as autophagy) plays a fundamental role in maintaining cellular homeostasis and survival [5], and impairment or inefficiencies in this degradation system are associated with the development of a variety of human diseases, ranging from neurodegenerative disorders to cancer [6,7]. Autophagy mediates degradation of a variety of substrates including proteinaceous aggregates (aggrephagy) [8], lipid droplets (lipophagy) [9], and organelles such as peroxisomes (pexophagy) [10]. Activation of the lysosome-autophagy system induced as a response to cellular internalization of nanomaterials may thus result in an increase in the cellular degradation capacity and enhanced clearance of endogenous materials [8,11,12]. The interaction of internalized nanomaterials with the lysosome-autophagy system, however, may also result in impairment of specific components of the pathway, such as the lysosome [13]. Clearance of autophagic cargo requires the fusion of autophagosomes with lysosomes to form autophagolysosomes where degradation occurs [14]. Both lysosomes and autophagosomes must be functionally active for transcriptional activation of the lysosome-autophagy system to translate into enhanced autophagic clearance [15]: indeed, defects

* Corresponding author at: Rice University, Department of Chemical and Biomolecular Engineering, 6100 Main St, MS-362, Houston, TX 77005, USA.
E-mail address: segatori@rice.edu (L. Segatori).

https://doi.org/10.1016/j.actbio.2018.08.021
1742-7061/

in the integrity and function of autophagosomes and lysosomes result in blockage of autophagic flux [16]. The effect of inorganic nanoparticles on lysosomal function and integrity, for instance, has been reported. The impairment of structural and functional integrity of lysosomes induced by nanoparticles may result in blockage of autophagic flux and accumulation of endogenous materials that are typically degraded *via* autophagy [16–20].

Titanium dioxide is "generally regarded as safe" by the US Food and Drug Administration [21]. While a number of personal care, biomedical, and industrial products contain titanium dioxide nanoparticles (TiO_2 NPs) [22], the effects of TiO_2 NPs on biological systems following cellular internalization remain unclear. A number of cellular pathways were found to be altered in association with cellular uptake of TiO_2 NPs including the oxidative stress response [23–26], inflammatory response [27], and lysosomal system [28]. Because the lysosome-autophagy system mediates the first cellular response to internalization of foreign nanomaterials, we investigated a comprehensive set of markers of the lysosome-autophagy system upon cellular exposure to TiO_2 NPs with primary particle diameters of 15, 50, and 100 nm. Results from this study provide important insights for the design of TiO_2 NPs with the desired effect on the lysosome-autophagy system, and ultimately, for engineering safe nanomaterial-containing products.

2. Materials and methods

2.1. Nanomaterial characterization studies

TiO_2 NPs were purchased from NanoAmor (5430MR, 15 nm) and mkNano (MK-TiO2-A050, 50 nm and MKN-TiO2-A100, 100 nm). TiO_2 nanopowders were prepared by the wet chemical synthesis method and present $\geq$98% TiO_2 purity, as specified by the manufacturer. Stock solutions (10 mg/mL) were prepared by suspending TiO_2 NPs in deionized water (18.2 MΩ-cm). Stock suspensions were sonicated immediately prior to use using a probe sonicator for 5 min at an 80% pulsation regime, stabilized with bovine serum albumin (BSA) through addition of an 80 mg/mL BSA-H_2O solution at a NP to protein mass ratio of 1:1, and further diluted in cell culture media immediately prior to use in biological assays [29].

Transmission electron microscopy (TEM) samples were prepared by dropping TiO_2 NP suspensions onto carbon type A 300 mesh copper grids. The TEM micrographs were taken using a JEOL 2010 TEM operated at 100 kV with a single tilt holder. The crystal structure and composition of the TiO_2 NPs were characterized by X-ray diffraction using a Rigaku D/Max Ultima II. Particle hydrodynamic diameter and zeta potential measurements (25 μg/mL) were obtained using a Beckman Coulter DelsaMax Pro system.

2.2. Cell cultures

HeLa cells (ATCC) were cultured in Dulbecco's Modified Eagle Medium (DMEM) supplemented with 10% fetal bovine serum (FBS) and 1% penicillin–streptomycin-glutamine (PSQ). HeLa cells overexpressing transcription factor EB (TFEB) fused to a FLAG tag (HeLa/TFEB cells) [30] were a gift from Dr. Marco Sardiello (Baylor College of Medicine). HeLa/TFEB cells were cultured in DMEM supplemented with 10% FBS and 1% PSQ and selected using G418 (1 mg/mL). H4/α-syn-GFP cells [31,32] were cultured in high glucose DMEM supplemented with 10% FBS and 1% PSQ and selected using blasticidin (5 μg/mL).

2.3. Immunofluorescence studies

Immunofluorescence studies were conducted as previously described [12,16]. Briefly, cells were seeded on glass coverslips in 12-well plates ($2{\cdot}10^4$ cell/well). HeLa/TFEB cells were cultured in the presence of TiO_2 NPs for 24 or 72 h. H4/α-syn-GFP cells were first transfected for the expression of TFEB-3XFLAG using the TFEB-3XFLAG plasmid from Dr. Marco Sardiello (Baylor College of Medicine), then cultured in the presence of TiO_2 NPs for 24 h. Cells were washed three times with PBS, fixed with 4% PFA (15 min), permeabilized with 0.1% Triton X-100 (10 min), and incubated with 8% BSA-PBS (30 min).

TFEB subcellular localization studies were conducted as previously described [33]. Cells were incubated with an anti-FLAG or anti-TFEB antibody (F7425, Sigma, 1:1000; ab70729, Abcam, 1:100) for one hour, washed, incubated with a fluorescent secondary antibody (611-142-002, Rockland, 1:500; 610-143-002, Rockland, 1:500) for one hour, washed, and then incubated with a Hoechst nuclear stain for ten minutes. Image post-processing and colocalization analyses were conducted using the JACoP plugin in ImageJ [34]. The fraction of nuclear TFEB was quantified by calculating the Mander's Overlap Coefficient for each image. Average values were calculated from analyses of ~50 cells per sample collected from at least three independent experiments. The percentage of cells presenting TFEB nuclear localization was determined by calculating the fraction of cells presenting the nuclear localization of TFEB as determined by evaluating the Mander's Overlap Coefficient greater than the average fraction of TFEB nuclear localization in untreated cells plus one standard deviation.

Lysosomal membrane permeabilization was evaluated by detecting lysosomal galectin-1 puncta as previously described [35]. Cells were incubated with anti-galectin-1 (ab25138, Abcam, 1:3000) and anti-lysosome-associated membrane protein-2 (LAMP-2, 354301, BioLegend, 1:2000) antibodies overnight at 4 °C, washed, and incubated with the appropriate fluorescent secondary antibodies (611-142-002, Rockland, 1:500; 072-03-15-06, KPL, 1:500) for one hour. Image post-processing was conducted using ImageJ to determine the number of LAMP-2-positive galectin-1 puncta on a cell-by-cell basis. Puncta were counted manually and average values were calculated by analyzing ~30 cells per sample from at least three independent experiments.

Microtubule-associated protein light chain 3 (LC3)-LAMP colocalization was evaluated as previously described [16]. Cells were incubated with anti-LC3 (NB100-2220, Novus Biologics, 1:1000) and anti-LAMP-2 (354301, BioLegend, 1:2000) antibodies for three hours, washed, and incubated with appropriate fluorescent secondary antibodies (611-143-002, Rockland, 1:500 or 610-142-002, Rockland, 1:500) for one hour. Image post-processing and colocalization analyses were conducted using the JACoP plugin in ImageJ [34]. The level of LC3-LAMP colocalization was quantified by calculating the Mander's Overlap Coefficient for each image. The number of LC3 puncta per cell was determined by thresholding images of LC3 and using the 'analyze particles' function in ImageJ.

2.4. Nanoparticle uptake studies

Cellular uptake of TiO_2 NPs was evaluated as previously described [36,37]. Briefly, HeLa/TFEB cells were plated in 12-well plates ($8{\cdot}10^4$ cell/well) and exposed to TiO_2 NPs for 24 h, washed three times with PBS, and collected in cell culture media. Uptake was quantified by measuring the side scattering parameter (SSC) of cells exposed to TiO_2 NPs using a BD FACSCanto II Flow Cytometer.

2.5. Cell viability analyses

Cellular membrane permeabilization was measured in HeLa/TFEB cells plated in 12-well plates ($8{\cdot}10^4$ cell/well) and cultured in media supplemented with TiO_2 NPs for 24, 48, or 72 h. Cells were collected in PBS and mixed with a 0.4% Trypan Blue solution

at a 1:1 volume ratio. At least 100 cells per biological replicate were counted using a hemocytometer, and the percentage of viable cells was determined using the following formula: % viable = 1 − (number of stained cells/total number of cells) × 100%.

Cellular metabolic activity was evaluated using the Promega CellTiter 96® AQueous One Solution Reagent. HeLa/TFEB cells were plated in 96-well plates ($5{\cdot}10^3$ cell/well) and cultured in media supplemented with TiO_2 NPs for 24 h. After exposure to TiO_2 NPs, 20 μL of the CellTiter 96® AQueous One Solution Reagent plus 100 μL of culturing media was pipetted into each well. Plates were incubated at 37 °C for 2 h in 5% CO_2. The amount of soluble formazan produced by the cellular reduction of 3-(4,5-dimethylthiazol-2-yl)-5-(3-carboxymethoxyphenyl)-2-(4-sulfophenyl)-2H-tetrazolium (MTS) was evaluated by measuring the absorbance of the solution at 490 nm using a Spectra Max Gemini EM Microplate Reader.

2.6. Western blot analyses

LC3 levels in HeLa cells were measured by plating cells in 10-cm dishes ($8{\cdot}10^5$ cell/dish, 24 h; $6{\cdot}10^5$ cell/dish, 72 h) and incubating with TiO_2 NPs for 24 or 72 h. Cells were collected and lysed with Complete Lysis-M buffer (Roche) containing a protease inhibitor cocktail. 40 μg of protein from each sample were separated by 15% SDS-PAGE. Membranes were incubated with primary antibodies (LC3, NB-100-2220, Novus Biologics, 1:1000; p62, 610832, BD Biosciences, 1:500; GAPDH, sc-25778, Santa Cruz Biotechnology, 1:10,000) and the appropriate secondary antibody (sc-2004, Santa Cruz Biotechnology, 1:12,000; sc-2005, Santa Cruz Biotechnology, 1:12,000). Imaging was performed on an LAS 4000 Imager and relative band densities were determined using ImageJ.

α-synuclein levels in H4/α-syn-GFP cells were measured by plating cells in 6-well plates ($20{\cdot}10^4$ cell/well) and incubating cells with TiO_2 NPs for 24 or 72 h. Cells were lysed using Complete Lysis-M buffer (Roche) containing a protease inhibitor cocktail and 1% Triton X-100 for 30 min on ice. Lysed cells were centrifuged for 60 mins at 15,000*g* and 4 °C, and the supernatant containing the soluble protein fraction was collected. The pellet was resuspended in Complete Lysis-M buffer supplemented with 2% SDS and 8 M urea and sonicated to collect the insoluble protein fraction. 4 μg of soluble protein and 40 μg of insoluble protein were separated by 12% SDS-PAGE for detection of α-synuclein and 40 μg of soluble protein for detection of LC3. Membranes were blotted using primary antibodies (α-synuclein, S5566, Sigma-Aldrich, 1:20,000; LC3, NB-100-2220, Novus Biologics, 1:1000; GAPDH, sc-25778, Santa Cruz Biotechnology, 1:10,000) and appropriate secondary antibodies (sc-2005, Santa Cruz Biotechnology, 1:12,000; sc-2004, Santa Cruz Biotechnology, 1:12,000). Imaging was performed on an LAS 4000 Imager and relative band densities were determined using ImageJ.

2.7. Statistical analyses

All data are presented as mean ± s.d. with the statistical significance calculated using a two-tailed Student's *t*-test unless stated otherwise. Differences are considered statistically significant with $^*p < 0.05$.

3. Results and discussion

3.1. TiO_2 NPs induce activation of the transcription factor EB

The autophagic response to TiO_2 NPs was investigated using a series of TiO_2 NPs with different primary particle diameters, namely 15, 50, and 100 nm (anatase crystal structure, Fig. 1A and B, Fig. S1). The hydrodynamic of diameter of each TiO_2 NP suspended in water or culturing media was first determined by dynamic light scattering (Fig. 1C). Media suspensions were prepared by sonicating water suspensions of TiO_2 NPs, stabilizing NPs through the addition of BSA, and diluting the resulting suspension in cell culture media (DMEM) [29]. Dynamic light scattering analyses suggest that the TiO_2 NPs form large agglomerates in water that are maintained upon dilution into DMEM, with the intermediate size of TiO_2 NPs tested (50 nm) forming the largest

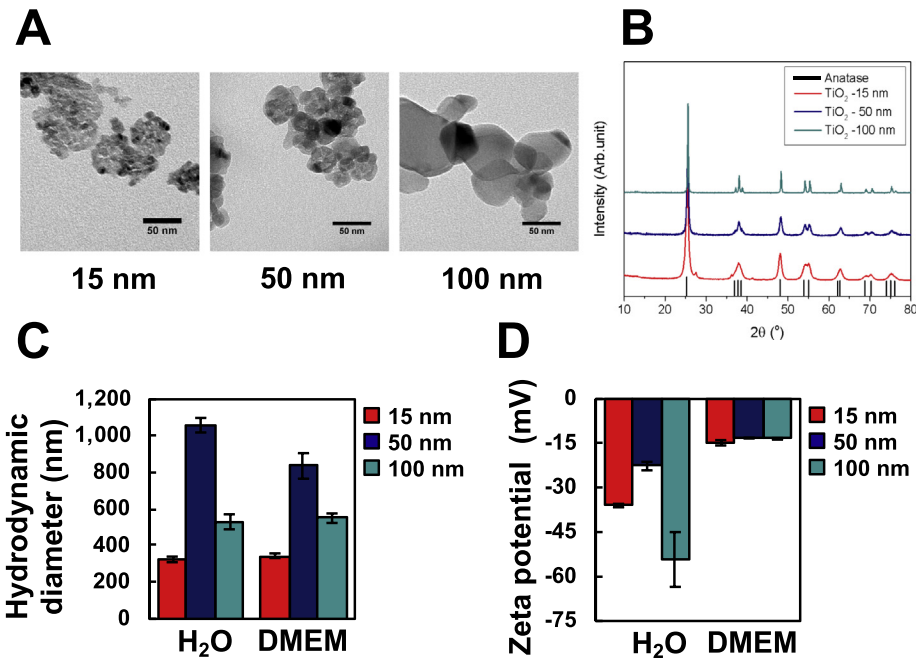

Fig. 1. Characterization of TiO_2 NPs. (A) TEM images of TiO_2 NPs dispersed in H_2O. Scale bar is 50 nm. (B) X-ray diffraction analyses of TiO_2 NPs. The anatase reference pattern is shown as vertical black lines (JCPDS Card #00-021-1272). (C-D) Dynamic light scattering analyses of the (C) hydrodynamic diameter and (D) zeta potential of TiO_2 NPs (25 μg/mL) dispersed in 1% BSA/H_2O or 1% BSA/DMEM. Data presented as mean ± s.d.

agglomerates (Fig. 1C; p-value <0.01). Zeta potential measurements of TiO_2 NPs revealed that all three TiO_2 NPs have a negative surface in solution with the 50 nm TiO_2 NPs presenting a more neutral surface charge in water compared to the 15 and 100 nm TiO_2 NPs (Fig. 1D). The more neutral surface charge of the 50 nm TiO_2 NPs in water compared to 10 and 100 nm TiO_2 NPs may reduce electrostatic repulsion and favor formation of larger agglomerates. While we did not observe a linear correlation between the TiO_2 NP primary particle diameters and their agglomerate size, the particles' properties, including surface area and volume, are still likely to play a significant role in the response of the lysosome-autophagy system [38,39]. In fact, TiO_2 NPs have been suggested to agglomerate and deagglomerate within cells, further implicating the importance of primary particle size on the cellular response to uptake of TiO_2 NPs [40]. Upon addition of BSA and dilution into DMEM, all three TiO_2 NPs exhibit similar, slightly negative zeta potentials most likely due to the formation of a protein corona [41].

To investigate the molecular mechanisms that mediate the autophagic response to TiO_2 NPs of different primary particle diameters, we first monitored the transcriptional regulatory network that controls induction of the lysosome-autophagy system by measuring activation of TFEB [42]. TFEB mediates integrated control of the lysosome-autophagy system by regulating the expression of the CLEAR (coordinated lysosomal expression and regulation) network [30,43]. This network includes genes that encode for lysosomal hydrolases, lysosomal membrane proteins, and autophagy-related proteins [43]. TFEB resides predominantly in the cytoplasm of cells under basal conditions and translocates into the nucleus upon activation [30]. We evaluated TFEB subcellular localization in HeLa cells stably transfected for the expression of TFEB-3XFLAG (HeLa/TFEB cells), as they provide an *in vitro* model system of TFEB activation [30]. HeLa/TFEB cells were cultured in DMEM supplemented with TiO_2 NPs (0–500 μg/mL; 24 h), and TFEB subcellular localization was monitored by immunofluorescence confocal microscopy using a Hoechst nuclear stain and an anti-FLAG antibody. TFEB activation was evaluated by calculating the Mander's Overlap Coefficient of the TFEB signal (anti-FLAG) and the nuclear stain (Fig. 2A, Fig. S2) and by determining the fraction of cells that present more nuclear TFEB than untreated cells (Fig. 2B) [34]. Colocalization analyses reveal that TFEB localizes predominantly in the cytoplasm of untreated HeLa/TFEB cells, as expected (Fig. 2A and B, white bars) [30]. Exposure of HeLa/TFEB cells to TiO_2 NPs was found to increase the fraction of TFEB that translocates into the nucleus. Specifically, we observed an increase in the fraction of nuclear TFEB (Fig. 2A) and in the number of cells presenting TFEB nuclear translocation (Fig. 2B) in cells exposed to 15 and 50 nm TiO_2 NPs at a media concentration of at least 50 μg/mL and in cells exposed to 100 nm TiO_2 NPs at a media concentration of at least 10 μg/mL. The extent of TFEB activation was found not to vary significantly as a function of primary particle size or particle agglomerate size. These results indicate that all three of the TiO_2 NPs induce activation of TFEB and that the extent of TFEB activation does not depend on the primary particle size.

To determine whether activation of TFEB in cells treated with TiO_2 NPs depends on the efficiency of cellular internalization, we evaluated the extent of TiO_2 NP uptake in HeLa/TFEB cells. Because TiO_2 NPs affect intracellular granularity [44], uptake was quantified by measuring the SSC of cells exposed to TiO_2 NPs (0–500 μg/mL; 24 h) using flow cytometry [36]. Internalization of the TiO_2 NPs was found to be concentration-dependent at low concentrations and to plateau at a TiO_2 NP media concentration of 200 μg/mL (Fig. 2C). The three TiO_2 NPs were found to exhibit similar uptake efficiency, suggesting that the primary particle diameter of the TiO_2 NPs used in this study does not affect TiO_2 NP uptake. To test whether uptake of the TiO_2 NPs induces cell toxicity, the viability of HeLa/TFEB cells treated with TiO_2 NPs under conditions that resulted in TFEB activation (0–500 μg/mL, 24–72 h) was investigated using the Trypan Blue dye exclusion technique (Fig. 2D–F). Similar results were obtained using the MTS assay (Fig. S3). We found that cellular exposure to the three TiO_2 NPs under the conditions used in this study does not cause a reduction in cell viability.

These results, taken together, indicate that cell exposure to TiO_2 NPs results in activation of TFEB, the master regulator of the lysosome-autophagy system, under conditions that do not affect cell viability. Furthermore, the extent of TiO_2 NP-induced TFEB activation does not depend on the primary particle size or agglomeration propensity of the TiO_2 NPs.

3.2. Cell exposure to TiO_2 NPs results in blockage of the autophagic flux

Biopersistent NPs, such as TiO_2 NPs [45], have been repeatedly reported to induce inactivation of lysosomal enzymes and destabilization of the lysosomal membrane, leading to impairment of autophagic clearance [13,16,46,47]. Interestingly, prolonged cellular exposure to TiO_2 NPs has been shown to affect lysosome acidification and lysosomal enzyme function [28,48]. To test the impact of the TiO_2 NPs used in this study on lysosomal integrity under conditions resulting in TFEB activation, we evaluated the extent of permeabilization of lysosomal membranes by monitoring lysosomal galectin puncta [35]. Galectins are soluble, carbohydrate-binding lectins that accumulate in the cytoplasm and rapidly translocate to leaky lysosomes [35]. Galectins bind to sites of lysosomal leakage due to the high concentration of β-galactosides found on the protective glycocalyx lining of lysosomal membranes that become exposed upon membrane permeabilization [49]. Lysosomal membrane permeabilization can thus be monitored by quantifying galectin puncta by immunofluorescence confocal microscopy [35]. HeLa/TFEB cells were exposed to TiO_2 NPs under conditions that result in TFEB activation (50, 100, and 500 μg/mL; 24 and 72 h). Cell treatment with L-leucyl-L-leucine methyl ester (2 mM, 2 h) was monitored as a positive control in this study [35] and was found to cause lysosomal membrane permeabilization in 49% of the cell population compared to untreated cells that were found not to present punctate galectin signal. Cell exposure to the 15, 50, and 100 nm TiO_2 NPs for a short time of incubation (50, 100, and 500 μg/mL; 24 h) did not result in the formation of punctate galectin signal (Fig. 3, white bars). Prolonged cell exposure to each of the three TiO_2 NPs (72 h), however, was found to cause lysosomal membrane permeabilization (Fig. 3, grey bars; Fig. S4). Specifically, we observed punctate galectin structures in about 20–40% of cells treated with each of the three types of TiO_2 NPs. The observed levels of lysosomal membrane permeabilization are not expected to cause considerable activation of cell death mechanisms [35]. These data suggest that prolonged exposure to TiO_2 NPs at concentrations that activate TFEB induces lysosomal membrane permeabilization.

Because autophagic clearance depends on fusion of lysosomes with autophagosomes, we asked whether cell treatment with TiO_2 NPs, under conditions that impair lysosomal integrity, would affect the turnover of autophagosomes. Autophagosome turnover was analyzed by measuring the intracellular levels of LC3.[50] LC3 is a soluble protein that accumulates in the cytoplasm under basal conditions.[51] Upon activation of autophagy, the cytosolic form of LC3 (LC3-I) is conjugated to phosphatidylethanolamine to form an LC3-phosphatidylethanolamine conjugate (LC3-II), which is recruited to autophagosomal membranes [51]. Fusion of autophagosomes with lysosomes results in formation of autophagolysosomes and degradation of autophagosomal components, including LC3-II, by lysosomal hydrolases; lysosomal turnover of the autophagosomal marker LC3-II thus reflects autophagic activity [50,52].

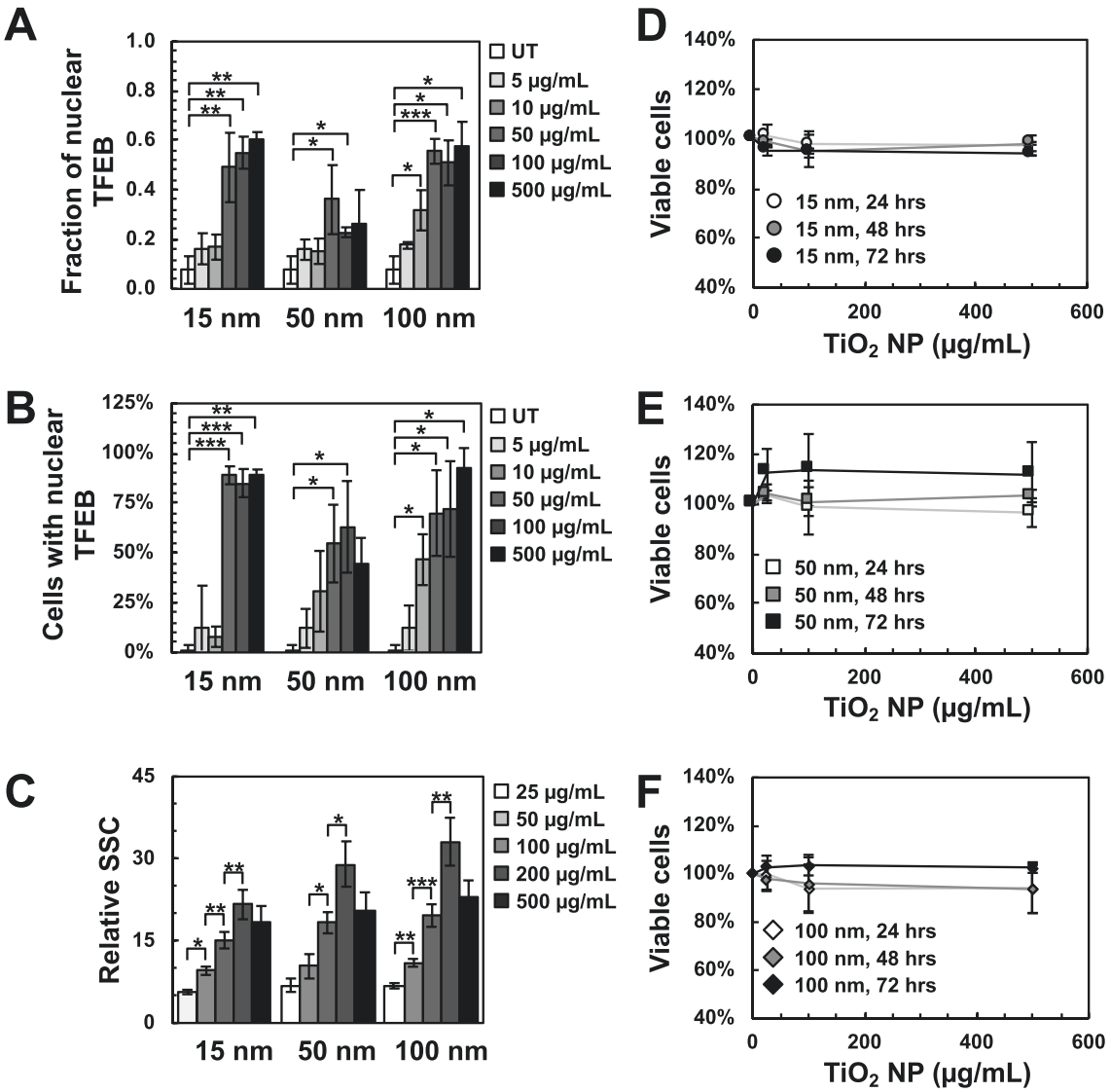

Fig. 2. TFEB activation in HeLa/TFEB cells exposed TiO_2 NPs. (A and B) Confocal microscopy analyses of TFEB in HeLa/TFEB cells incubated with TiO_2 NPs for 24 h. (A) Average fraction of total cellular TFEB that localizes in the nucleus. UT, untreated. Data presented as mean ± s.e.m. $^{*}p < 0.05$, $^{**}p < 0.01$, $^{***}p < 0.001$. (B) Percentage of HeLa/TFEB cells with fraction of nuclear TFEB greater than average fraction of nuclear TFEB in untreated cells. UT, untreated. Data presented as mean ± s.e.m. $^{*}p < 0.05$, $^{**}p < 0.01$, $^{***}p < 0.001$. (C) Side scattering parameter (SSC) of HeLa/TFEB cells exposed to TiO_2 NPs for 24 h measured by flow cytometry. Relative SSC values were calculated by normalizing the SSC of treated cells to untreated cells. Data presented as mean ± s.d. $^{*}p < 0.05$, $^{**}p < 0.01$, $^{***}p < 0.001$. (D–F) Viability of HeLa/TFEB cells treated with TiO_2 NPs for 24, 48, and 72 h. Data presented as mean ± s.d.

The effect of short (24 h) and prolonged (72 h) exposure of HeLa cells to TiO_2 NPs on autophagosome accumulation was evaluated by testing the levels of LC3-I and LC3-II by immunoblotting. We observed a concentration-dependent increase in the LC3-II/LC3-I ratio after 24 h of treatment with 15, 50, and 100 nm TiO_2 NPs, suggesting formation of autophagosomes (Fig. 4, Fig. S5). Addition of bafilomycin (10 nM; 1 h), a selective inhibitor of vacuolar H+ ATPases that is known to block autophagic flux [15], was found to increase the LC3-II/LC3-I ratio in cells exposed to low concentrations of TiO_2 NPs (10 µg/mL; 24 h) but not in cells exposed to high concentrations of TiO_2 NPs (100 µg/mL; 24 h) (Fig. 4A–C, Fig. S5A–C). These results suggest that short exposure to low concentrations of TiO_2 NPs results in enhancement of autophagic activity without accumulation of autophagosomes, while increasing the concentration of TiO_2 NPs in the culturing media causes accumulation of autophagosomes, which is typically associated with blockage of autophagic flux. Interestingly, accumulation of autophagosomes was also observed upon prolonged cell exposure to even low media TiO_2 NP concentrations (10 µg/mL) (Fig. 4D–F, Fig. S5D–F), again indicative of a blockage of autophagic flux. In summary, analyses of LC3 levels indicate that cell exposure to TiO_2 NPs induces the

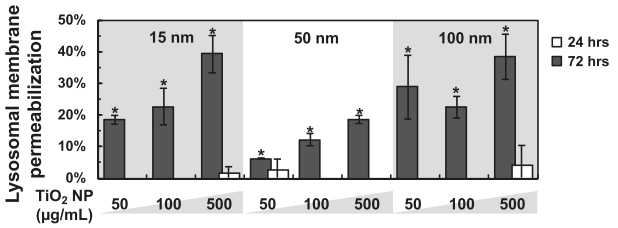

Fig. 3. Lysosomal membrane permeabilization in HeLa/TFEB cells exposed to TiO_2 NPs. Permeabilization of lysosomal membranes in HeLa/TFEB cells incubated with TiO_2 NPs (50, 100, or 500 µg/mL; 24 or 72 h) as measured by confocal microscopy analyses of galectin-1 and lysosome-associated membrane protein-2 (LAMP-2). Data presented as mean ± s.e.m. $^{*}p < 0.05$.

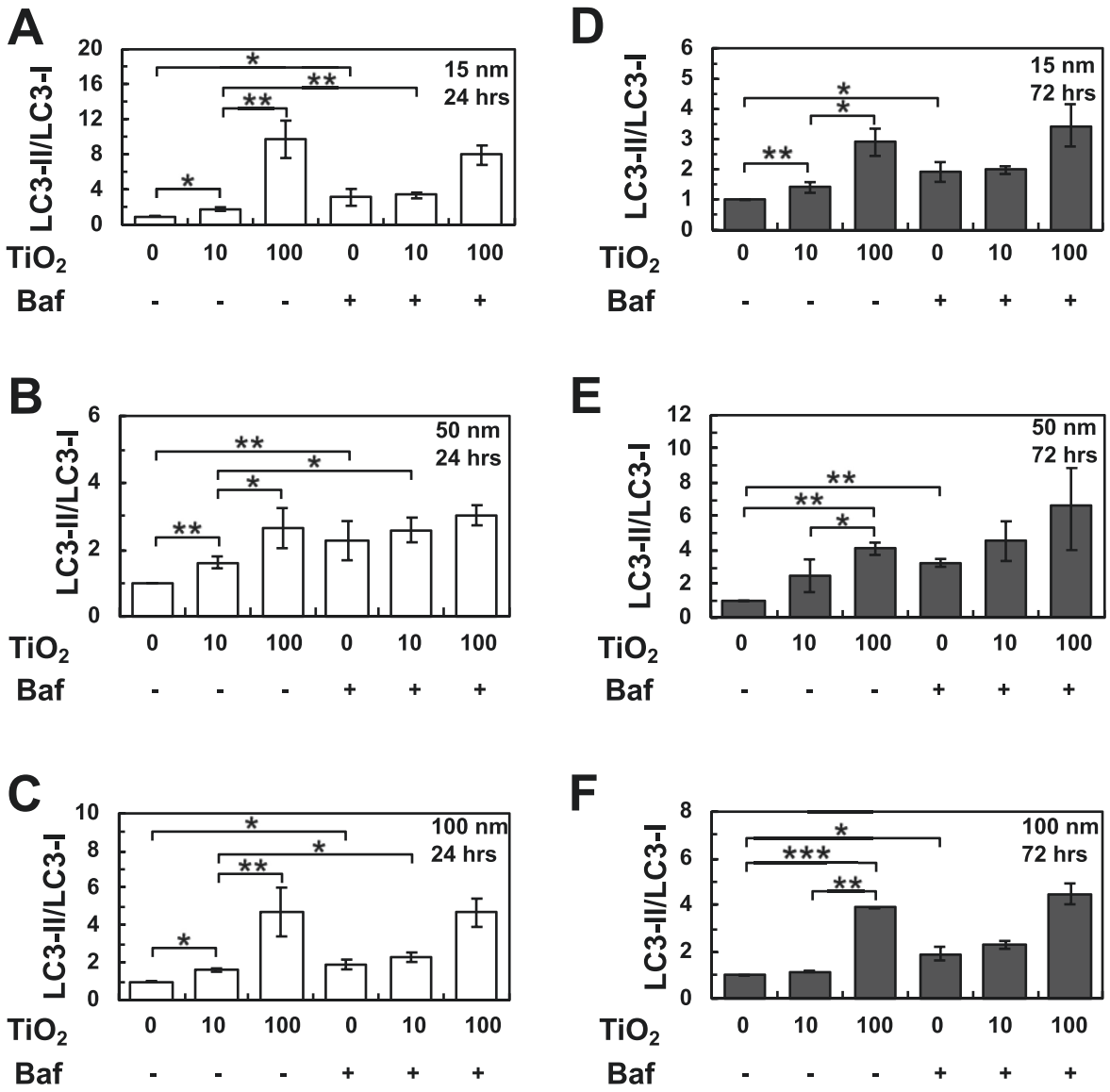

Fig. 4. LC3 protein expression levels and processing in HeLa cells exposed to TiO_2 NPs. LC3 levels in HeLa cells incubated with TiO_2 NPs (10 or 100 μg/mL) for (A–C) 24 h or (D–F) 72 h and in the presence of bafilomycin (10 nM; 1 h) determined by Western blot and reported as ratio of autophagosomal (LC3-II) to cytoplasmic (LC3-I) isoforms. Data presented as mean ± s.d. $^{*}p < 0.05$, $^{**}p < 0.01$, $^{***}p < 0.001$. Baf, bafilomycin.

formation of autophagosomes in a concentration-dependent manner, with prolonged exposure to TiO_2 NPs inducing accumulation of autophagosomes. The observed increase in accumulation of autophagosomes parallels the increase in permeabilization of lysosomal membranes, suggesting that autophagosomal accumulation is likely to be associated with lysosomal impairment and blockage of autophagic flux.

The effect of short (24 h) and prolonged (72 h) exposure of HeLa cells to TiO_2 NPs (10 or 100 μg/mL) on autophagosome formation and turnover was also evaluated by testing the levels of p62 (also known as SQSTM1) in the presence or absence of bafilomycin (Figs. S6 and S7). Western blot analyses revealed a mild increase in the levels of p62 in HeLa cells exposed to TiO_2 NPs for 24 h (Figs. S6A and S7A) compared to untreated cells. We speculate that TiO_2 NPs may agglomerate within the cytoplasm of treated cells and be tagged with p62 for recognition by the autophagy system. This response typically leads to an increase in the levels of p62, which mediates delivery of intracellular cargo into autophagosomes [53]. The notion that sequestration of different types of nanomaterials into autophagosomes, similar to the sequestration of intracellular pathogenic bacteria, may be mediated by p62 was recently reported [13,54,55]. Bafilomycin prevents autophagic degradation of p62 that has been recruited to autophagic structures [53]. Addition of bafilomycin to cells exposed to TiO_2 NPs for 24 h led to a further increase in p62 levels, confirming that short exposure to TiO_2 NPs does not cause blockage of autophagic flux. Addition of bafilomycin to cells exposed to TiO_2 NPs for 72 h, however, did not alter the levels of p62 (Fig. 4), confirming that prolonged exposure causes blockage of the autophagic flux.

The autophagic flux can be further monitored by correlating the intracellular levels of LC3 (autophagosome formation) with colocalization of LC3 with the lysosomal membrane protein LAMP-2 (autophagolysosome formation) [56,57]. Low levels of LC3 and LC3-LAMP colocalization are typically indicative of basal autophagic activity. An increase in LC3 levels that is not paralleled by an increase in LC3-LAMP colocalization indicates a block in autophagic flux, while an increase in LC3 levels that is paralleled by an increase in LC3-LAMP colocalization is characteristic of enhanced autophagic flux [57].

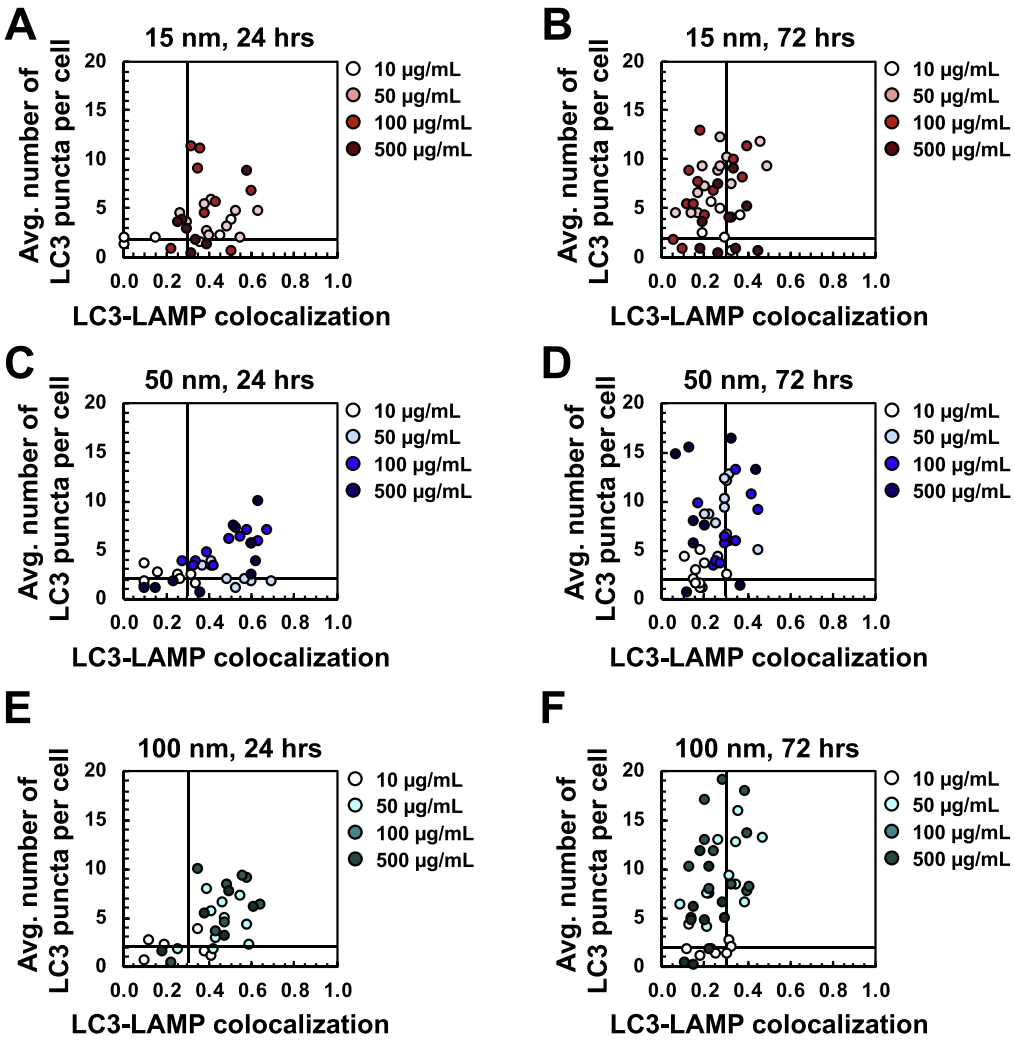

Fig. 5. LC3-LAMP colocalization in HeLa/TFEB cells exposed to TiO_2 NPs. Quantification of the average number of LC3 puncta per cell and colocalization of LC3 and LAMP-2 in HeLa/TFEB cells incubated with 15, 50, and 100 nm TiO_2 NPs (10, 50, 100, and 500 μg/mL; 24 or 72 h) determined by confocal microscopy. Data points represent images of 10–20 cells. The average basal level of LC3-LAMP colocalization (0.30 ± 0.02) and LC3 puncta/cell (1.9 ± 0.3) of untreated cells are reported as solid black lines.

HeLa/TFEB cells were treated with TiO_2 NPs (10, 50, 100, and 500 μg/mL; 24 or 72 h) and immunofluorescence confocal microscopy images were analyzed to quantify the number of LC3 puncta per cell and the extent of colocalization of LC3 and LAMP (Fig. 5, Figs. S8–S10). Cells treated with TiO_2 NPs at concentrations greater than 10 μg/mL for a short time of exposure (24 h) were predominantly characterized by an increase in both the average number of LC3 puncta per cell and the extent of LC3-LAMP colocalization, a pattern indicative of an increase in autophagic vesicles and enhanced autophagic flux. Cells treated with 10 μg/mL TiO_2 NPs exhibited minimal changes in LC3 puncta and LC3-LAMP colocalization compared with untreated cells. Prolonged exposure to TiO_2 NPs (72 h) resulted in an increase in the average number of LC3 puncta per cell that does not parallel an increase in LC3-LAMP colocalization. The high levels of autophagosomal markers associated with a level of formation of autophagolysosomes comparable to untreated cells observed upon prolonged exposure to TiO_2 NPs is indicative of blockage of autophagic flux, likely due to accumulation of autophagosomes that do not fuse with lysosomes to form autophagolysosomes.

These results, taken together, suggest that prolonged exposure to the three TiO_2 NPs used in this study leads to lysosomal membrane permeabilization and autophagosome accumulation, resulting in a blockage of autophagic flux, and that this TiO_2 NP-mediated effect on the lysosome-autophagy system is independent of the primary particle size and particle agglomerate size of the TiO_2 NPs.

3.3. Prolonged exposure to TiO_2 NPs impairs clearance of autophagic substrates

To test whether TiO_2 NP-induced activation of autophagy results in enhanced clearance of autophagic cargo, we monitored the intracellular accumulation of aggregated α-synuclein, which is a model substrate of autophagic clearance [8]. Specifically, we tested the accumulation of aggregated α-synuclein in human H4 neuroglioma cells engineered to express α-synuclein fused to GFP (H4/α-syn-GFP) [31,32] exposed to TiO_2 NPs. H4/α-syn-GFP cells were first transfected to express TFEB-3XFLAG to evaluate the extent of TFEB activation induced by exposure to TiO_2 NPs. Transfected cells were incubated with 15, 50, and 100 nm TiO_2 NPs (100 μg/mL; 24 h). Confocal microscopy analyses show that TFEB is predominately found in the cytoplasm of untreated cells and in the nucleus of cells treated with the TiO_2 NPs, indicating that exposure of H4/α-syn-GFP cells to TiO_2 NPs leads to transcriptional activation of autophagy (Fig. 6A). Exposure of H4/α-syn-GFP cells to TiO_2 NPs (100 μg/mL, 24 or 72 h) was also found to increase LC3-II/LC3-I levels (Fig. 6B, Fig. S11), confirming activation of

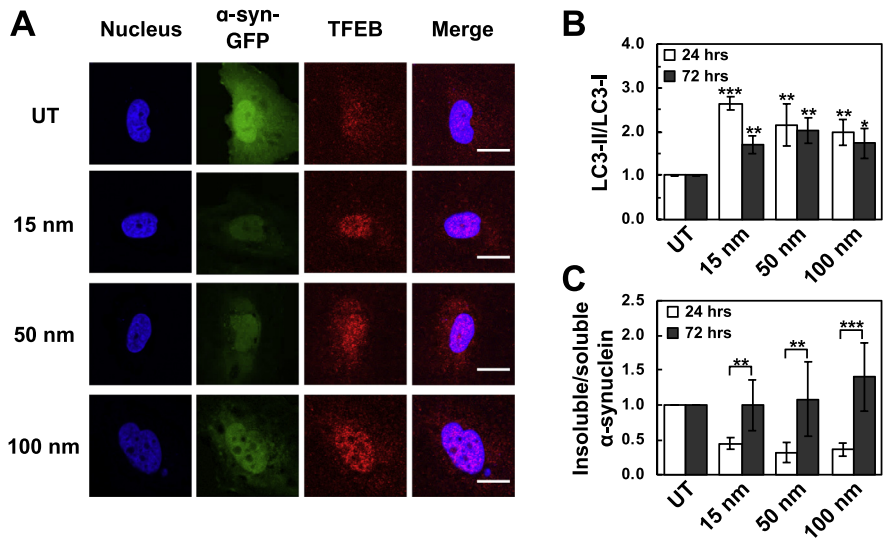

Fig. 6. Accumulation of autophagic substrates in H4/α-syn-GFP cells exposed to TiO_2 NPs. (A) Confocal microscopy analyses of TFEB subcellular localization in H4/α-syn-GFP cells transfected with TFEB-3XFLAG and incubated with TiO_2 NPs (100 μg/mL, 24 h). Representative images of colocalization of nuclei (blue, Hoechst stain, column 1) and TFEB (red, anti-TFEB, column 3) is shown in merged images (column 4). Scale bar is 20 μm. (B) Quantification of LC3-II/LC3-I levels in the soluble protein fraction of H4/α-syn-GFP cells treated with TiO_2 NPs (100 μg/mL; 24 or 72 h) measured by Western blot. Data presented as mean ± s.d. $^{*}p < 0.05$, $^{**}p < 0.01$, $^{***}p < 0.001$. (C) Quantification of α-synuclein levels in soluble and insoluble protein fractions of H4/α-syn-GFP cells treated with TiO_2 NPs (100 μg/mL; 24 or 72 h) determined by Western blot. Data are presented as mean ± s.d. $^{*}p < 0.05$, $^{**}p < 0.01$. (For interpretation of the references to colour in this figure legend, the reader is referred to the web version of this article.)

autophagy and formation of autophagic vesicles. The effect of TiO_2 NPs on autophagic clearance was evaluated by quantifying the amount of soluble and insoluble α-synuclein in H4/α-syn-GFP cells treated with TiO_2 NPs (100 μg/mL; 24 or 72 h) by Western blot (Fig. 6C, Fig. S11) [8]. Short exposure (24 h) to the TiO_2 NPs was found to result in a reduction in the ratio of insoluble to soluble α-synuclein (Fig. 6C, Fig. S11A and B), suggesting that TiO_2 NP-induced activation of autophagy enhances the clearance of α-synuclein aggregates. The ratio of insoluble to soluble levels of α-synuclein in cells exposed to TiO_2 NPs for prolonged times (72 h) were found to be comparable to, or higher than, that of untreated cells (Fig. 6C, Fig. S11C and D), suggesting that activation of the autophagic response does not parallel enhanced clearance upon prolonged exposure to TiO_2 NPs, and may instead result in blockage in autophagic flux and accumulation of autophagic cargo.

4. Conclusions

An increase in the number of individuals being exposed to engineered nanomaterials has resulted in an urgent need to characterize the interaction of nanomaterials with biological systems and to understand the effect of nano-bio interactions on cellular components, which also operate at the nanoscale. Cellular internalization of nanomaterials results in activation of the lysosome-autophagy system, most likely as the cellular response to what it is perceived as foreign or toxic [13,58]. Depending on their specific physicochemical properties, however, nanomaterials may also have adverse effects on components of the lysosome-autophagy system. Inorganic nanoparticles, for instance, may affect lysosomal integrity and function, which, in turn, may have an effect on autophagic degradation [13].

This study provides a comprehensive analysis of the autophagy-inducing properties of three TiO_2 NPs of anatase crystal structure with varying primary particle sizes (15, 50, and 100 nm). Specifically, the effects of TiO_2 NP uptake on the autophagy pathway was assessed by monitoring regulation of the lysosome-autophagy system at the transcriptional level, formation of autophagic vesicles and fusion of autophagic vesicles with lysosomes, and, ultimately, clearance of endogenous autophagic substrates. We report that the cellular uptake of TiO_2 NPs results in activation of the lysosome-autophagy system *via* TFEB. We also found that prolonged exposure to TiO_2 NPs results in lysosomal dysfunction and lysosomal membrane permeabilization, which leads to a blockage in autophagic flux. Our results point to a minimal effect of the primary particle size on the autophagic response under the experimental conditions used in this study. It remains to be determined whether agglomeration of TiO_2 NPs affects the interaction of this nanomaterial with the lysosome-autophagy system and whether the size of the resulting agglomerates plays a role in shaping the response of this important homeostatic pathway to cellular internalization of TiO_2 based nanoparticles. Furthermore, while this study provides an experimental pipeline for monitoring the lysosome-autophagy system upon uptake of TiO_2 NPs and provides important insights on the cellular and molecular mechanisms underlying the autophagic response to TiO_2 NPs, it remains important to extend the approaches reported herein to other *in vitro* systems of biomedical relevance, as cancerous cell lines may have higher basal levels of autophagy than primary cells [59,60].

Acknowledgements

This work was funded by The National Science Foundation (CBET-1615562 and CBET-1805317) and the Welch Foundation (C-1824). We greatly appreciate Santiago Martinez Legaspi (Chemical and Biomolecular Engineering, Rice University) and Dr. Nasim Taheri (Chemistry, Rice University) for providing TEM images and X-ray diffraction data, respectively.

Appendix A. Supplementary data

Supplementary data associated with this article can be found, in the online version, at https://doi.org/10.1016/j.actbio.2018.08.021.

References

[1] M.R. Mohammadi, A. Nojoomi, M. Mozafari, A. Dubnika, M. Inayathullah, J. Rajadas, Nanomaterials engineering for drug delivery: a hybridization approach, J. Mater. Chem. B. 5 (2017) 3995–4018, https://doi.org/10.1039/C6TB03247H.

[2] P.D. Howes, R. Chandrawati, M.M. Stevens, Colloidal nanoparticles as advanced biological sensors, Science 346 (80-) (2014) 1247390, https://doi.org/10.1126/science.1247390.
[3] M.E. Vance, T. Kuiken, E.P. Vejerano, S.P. McGinnis, M.F. Hochella, D.R. Hull, Nanotechnology in the real world: Redeveloping the nanomaterial consumer products inventory, Beilstein J. Nanotechnol. 6 (2015) 1769–1780, https://doi.org/10.3762/bjnano.6.181.
[4] R. Diaz-Torres, R. Lopez-Arellano, J. Escobar-Chavez, E. Garcıa-Garcia, C.L. Dominguez-Delgado, P. Ramirez-Noguera, Effect of size and functionalization of pharmaceutical nanoparticles and their interaction with biological systems, in: M. Aliofkhazraei (Ed.), Handb. Nanoparticles, Springer R, 2016, pp. 1040–1060, https://doi.org/10.1007/978-3-319-15338-4.
[5] P. Boya, F. Reggiori, P. Codogno, Emerging regulation and functions of autophagy, Nat. Cell Biol. 15 (2013) 713–720, https://doi.org/10.1038/ncb2788.
[6] A.M.K. Choi, S.W. Ryter, B. Levine, Autophagy in human health and disease, N. Engl. J. Med. 368 (2013) 651–662, https://doi.org/10.1056/NEJMra1205406.
[7] C.C. Tan, J.T. Yu, M.S. Tan, T. Jiang, X.C. Zhu, L. Tan, Autophagy in aging and neurodegenerative diseases: Implications for pathogenesis and therapy, Neurobiol. Aging 35 (2014) 941–957, https://doi.org/10.1016/j.neurobiolaging.2013.11.019.
[8] K. Kilpatrick, Y. Zeng, T. Hancock, L. Segatori, Genetic and chemical activation of TFEB mediates clearance of aggregated α-synuclein, PLoS One 10 (2015) e0120819.
[9] K. Liu, M.J. Czaja, Regulation of lipid stores and metabolism by lipophagy, Cell Death Differ. 20 (2013) 3–11, https://doi.org/10.1038/cdd.2012.63.
[10] J. Zhang, D.N. Tripathi, J. Jing, A. Alexander, J. Kim, T. Powell, R. Dere, J. Tait-mulder, J. Lee, T.T. Paull, K. Raj, V.K. Charaka, T.K. Pandita, M.B. Kastan, C. Lyn, ATM functions at the peroxisome to induce pexophagy in response to ROS, Nat. Cell Biol. 17 (2015) 1259–1269, https://doi.org/10.1038/ncb3230.ATM.
[11] W. Song, F. Wang, P. Lotfi, M. Sardiello, L. Segatori, 2-hydroxypropyl-beta-cyclodextrin promotes TFEB-mediated activation of autophagy: implications for therapy, J. Biol. Chem. 289 (2014) 10211–10222, https://doi.org/10.1074/jbc.M113.506246.
[12] W. Song, S.S. Lee, M. Savini, L. Popp, V.L. Colvin, L. Segatori, Ceria nanoparticles stabilized by organic surface coatings activate the lysosome-autophagy system and enhance autophagic clearance, ACS Nano. 8 (2014) 10328–10342, https://doi.org/10.1021/nn505073u.
[13] S.T. Stern, P.P. Adiseshaiah, R.M. Crist, Autophagy and lysosomal dysfunction as emerging mechanisms of nanomaterial toxicity, Part. Fibre Toxicol. 9 (2012) 20, https://doi.org/10.1186/1743-8977-9-20.
[14] A. Lieberman, R. Puertollano, N. Raben, S. Slaugenhaupt, S. Walkley, A. Ballabio, Autophagy in lysosomal storage disorders, Autophagy 8 (2012) 719–730.
[15] A. Yamamoto, Y. Tagawa, T. Yoshimori, Y. Moriyama, R. Masaki, Y. Tashiro, Bafilomycin A1 prevents maturation of autophagic vacuoles by inhibiting fusion between autophagosomes and lysosomes in rat hepatoma cell line, H-4-II-E cells, Cell Struct. Funct. 23 (1998) 33–42.
[16] W. Song, L. Popp, J. Yang, A. Kumar, V.S. Gangoli, L. Segatori, The autophagic response to polystyrene nanoparticles is mediated by transcription factor EB and depends on surface charge, J. Nanobiotechnol. 13 (2015) 87, https://doi.org/10.1186/s12951-015-0149-6.
[17] D.N. Johnson-Lyles, K. Peifley, S. Lockett, B.W. Neun, M. Hansen, J. Clogston, S.T. Stern, S.E. McNeil, Fullerenol cytotoxicity in kidney cells is associated with cytoskeleton disruption, autophagic vacuole accumulation, and mitochondrial dysfunction, Toxicol. Appl. Pharmacol. 248 (2010) 249–258, https://doi.org/10.1016/j.taap.2010.08.008.
[18] Y.-H. Lee, F.-Y. Cheng, H.-W. Chiu, J.-C. Tsai, C.-Y. Fang, C.-W. Chen, Y.-J. Wang, Cytotoxicity, oxidative stress, apoptosis and the autophagic effects of silver nanoparticles in mouse embryonic fibroblasts, Biomaterials 35 (2014) 4706–4715, https://doi.org/10.1016/j.biomaterials.2014.02.021.
[19] X. Ma, Y. Wu, S. Jin, Y. Tian, X. Zhang, Y. Zhao, L. Yu, X.-J. Liang, Gold nanoparticles induce autophagosome accumulation through size-dependent nanoparticle uptake and lysosome impairment, ACS Nano 5 (2011) 8629–8639, https://doi.org/10.1021/nn202155y.
[20] R. Li, Z. Ji, H. Qin, X. Kang, B. Sun, M. Wang, C.H. Chang, X. Wang, H. Zhang, H. Zou, A.E. Nel, T. Xia, Interference in autophagosome fusion by rare earth nanoparticles disrupts autophagic flux and regulation of an interleukin-1 β producing inflammasome, ACS Nano 8 (2014) 10280–10292.
[21] Title 21: Food and Drugs, in: Code Fed. Regul., 2015, p. §73.575, §73.1575, §73.2575, §73.3126.
[22] A. Weir, P. Westerhoff, L. Fabricius, K. Hristovski, N. von Goetz, Titanium dioxide nanoparticles in food and personal care products, Environ. Sci. Technol. 46 (2012) 2242–2250, https://doi.org/10.1021/es204168d.
[23] S. Hussain, S. Boland, A. Baeza-Squiban, R. Hamel, L.C.J. Thomassen, J. Martens, M.A. Billon-Galland, J. Fleury-Feith, F. Moisan, J.-C. Pairon, F. Marano, Oxidative stress and proinflammatory effects of carbon black and titanium dioxide nanoparticles: role of particle surface area and internalized amount, Toxicology 260 (2009) 142–149, https://doi.org/10.1016/j.tox.2009.04.001.
[24] I. De Angelis, F. Barone, A. Zijno, L. Bizzarri, M.T. Russo, R. Pozzi, F. Franchini, G. Giudetti, C. Uboldi, J. Ponti, F. Rossi, B. De Berardis, Comparative study of ZnO and TiO2 nanoparticles: physico-chemical characterization and toxicological effects on human colon carcinoma cells, Nanotoxicology 7 (2012) 1–40, https://doi.org/10.3109/17435390.2012.741724.
[25] C.Y. Tay, W. Fang, M.I. Setyawati, S.L. Chia, K.S. Tan, C. Hsu, L. Hong, D.T. Leong, Nano-hydroxyapatite and nano-titanium dioxide exhibit different subcellular distribution and apoptotic profile in human oral epithelium, ACS Appl. Mater. Interfaces 6 (2014) 6248–6256.
[26] K. Bhattacharya, M. Davoren, J. Boertz, R.P. Schins, E. Hoffmann, E. Dopp, Titanium dioxide nanoparticles induce oxidative stress and DNA-adduct formation but not DNA-breakage in human lung cells, Part. Fibre Toxicol. 6 (2009) 17, https://doi.org/10.1186/1743-8977-6-17.
[27] S.G. Han, B. Newsome, B. Hennig, Titanium dioxide nanoparticles increase inflammatory responses in vascular endothelial cells, Toxicology 306 (2013) 1–8, https://doi.org/10.1016/j.tox.2013.01.014.
[28] S. Hussain, L.C.J. Thomassen, I. Ferecatu, M.-C. Borot, K. Andreau, J. Martens, J. Fleury, A. Baeza-Squiban, F. Marano, S. Boland, Carbon black and titanium dioxide nanoparticles elicit distinct apoptotic pathways in bronchial epithelial cells, Part. Fibre Toxicol. 7 (2010) 10, https://doi.org/10.1186/1743-8977-7-10.
[29] J.S. Taurozzi, V.A. Hackley, M.R. Wiesner, A standardised approach for the dispersion of titanium dioxide nanoparticles in biological media, Nanotoxicology 7 (2013) 389–401, https://doi.org/10.3109/17435390.2012.665506.
[30] M. Sardiello, M. Palmieri, A. di Ronza, D.L. Medina, M. Valenza, V.A. Gennarino, C. Di Malta, F. Donaudy, V. Embrione, R.S. Polishchuk, S. Banfi, G. Parenti, E. Cattaneo, A. Ballabio, A gene network regulating lysosomal biogenesis and function, Science 325 (2009) 473–477, https://doi.org/10.1126/science.1174447.
[31] N.P. Cook, K. Kilpatrick, L. Segatori, A.A. Martí, Detection of α-synuclein amyloidogenic aggregates in vitro and in cells using light-switching dipyridophenazine ruthenium(II) complexes, J. Am. Chem. Soc. 134 (2012) 20776–20782, https://doi.org/10.1021/ja3100287.
[32] K. Kilpatrick, J.A. Novoa, T. Hancock, C.J. Guerriero, P. Wipf, J.L. Brodsky, L. Segatori, Chemical induction of Hsp70 reduces α-synuclein aggregation in neuroglioma cells, ACS Chem. Biol. 8 (2013) 1460–1468, https://doi.org/10.1021/cb400017h.
[33] L. Popp, E. Gomez, W. Orji, M. Ho, J. Suh, L. Segatori, TFEB-mediated activation of the lysosome-autophagy system affects the transduction efficiency of adeno-associated virus 2, Virology 510 (2017) 1–8, https://doi.org/10.1016/j.virol.2017.06.030.
[34] S. Bolte, F.P. Cordelieres, A guided tour into subcellular colocalisation analysis in light microscopy, J. Microsc. 224 (2006) 213–232.
[35] S. Aits, J. Kricker, B. Liu, A.-M. Ellegaard, S. Hämälistö, S. Tvingsholm, E. Corcelle-Termeau, S. Høgh, T. Farkas, A.H. Jonassen, I. Gromova, M. Mortensen, M. Jäättelä, Sensitive detection of lysosomal membrane permeabilization by lysosomal galectin puncta assay, Autophagy 11 (2015) 1408–1424, https://doi.org/10.1080/15548627.2015.1063871.
[36] Y. Ibuki, T. Toyooka, Nanoparticle uptake measured by flow cytometry, Methods Mol. Biol. 926 (2012) 157–166, https://doi.org/10.1007/978-1-62703-002-1_11.
[37] H. Suzuki, T. Toyooka, Y. Ibuki, Simple and easy method to evaluate uptake potential of nanoparticles in mammalian cells using a flow cytometric light scatter analysis, Environ. Sci. Technol. 41 (2007) 3018–3024.
[38] D. Huang, H. Zhou, J. Gao, Nanoparticles modulate autophagic effect in a dispersity-dependent manner, Sci. Rep. 5 (2015) 1–11, https://doi.org/10.1038/srep14361.
[39] A. Albanese, P.S. Tang, W.C.W. Chan, The effect of nanoparticle size, shape, and surface chemistry on biological systems, Annu. Rev. Biomed. Eng. 14 (2012) 1–16, https://doi.org/10.1146/annurev-bioeng-071811-150124.
[40] L. Ahlinder, B. Ekstrand-Hammarström, P. Geladi, L. Österlund, Large uptake of titania and iron oxide nanoparticles in the nucleus of lung epithelial cells as measured by raman imaging and multivariate classification, Biophys. J. 105 (2013) 310–319, https://doi.org/10.1016/J.BPJ.2013.06.017.
[41] H.-W. Chiu, T. Xia, Y.-H. Lee, C.-W. Chen, J.-C. Tsai, Y.-J. Wang, Cationic polystyrene nanospheres induce autophagic cell death through the induction of endoplasmic reticulum stress, Nanoscale 7 (2015) 736–746, https://doi.org/10.1039/C4NR05509H.
[42] C. Settembre, A. Ballabio, TFEB regulates autophagy: An integrated coordination of cellular degradation and recycling processes, Autophagy 7 (2011) 1379–1381.
[43] M. Palmieri, S. Impey, H. Kang, A. di Ronza, C. Pelz, M. Sardiello, A. Ballabio, Characterization of the CLEAR network reveals an integrated control of cellular clearance pathways, Hum. Mol. Genet. 20 (2011) 3852–3866, https://doi.org/10.1093/hmg/ddr306.
[44] R.M. Zucker, E.J. Massaro, K.M. Sanders, L.L. Degn, W.K. Boyes, Detection of TiO2 nanoparticles in cells by flow cytometry, Cytometry A 77 (2010) 677–685, https://doi.org/10.1002/cyto.a.20927.
[45] L. Gate, C. Disdier, F. Cosnier, F. Gagnaire, J. Devoy, W. Saba, E. Brun, M. Chalansonnet, A. Mabondzo, Biopersistence and translocation to extrapulmonary organs of titanium dioxide nanoparticles after subacute inhalation exposure to aerosol in adult and elderly rats, Toxicol. Lett. 265 (2017) 61–69, https://doi.org/10.1016/j.toxlet.2016.11.009.
[46] W.-S. Cho, R. Duffin, S.E.M. Howie, C.J. Scotton, W.A.H. Wallace, W. Macnee, M. Bradley, I.L. Megson, K. Donaldson, Progressive severe lung injury by zinc oxide nanoparticles; the role of Zn2+ dissolution inside lysosomes, Part Fibre Toxicol. 8 (2011) 27, https://doi.org/10.1186/1743-8977-8-27.
[47] M. Yang, M. Zhang, Y. Tahara, S. Chechetka, E. Miyako, S. Iijima, M. Yudasaka, Lysosomal membrane permeabilization: Carbon nanohorn-induced reactive oxygen species generation and toxicity by this neglected mechanism, Toxicol. Appl. Pharmacol. 280 (2014) 117–126, https://doi.org/10.1016/j.taap.2014.07.022.
[48] E. Moschini, M. Gualtieri, M. Colombo, U. Fascio, M. Camatini, P. Mantecca, The modality of cell-particle interactions drives the toxicity of nanosized CuO and

TiO_2 in human alveolar epithelial cells, Toxicol. Lett. 222 (2013) 102–116, https://doi.org/10.1016/j.toxlet.2013.07.019.
[49] C. Settembre, A. Fraldi, D.L. Medina, A. Ballabio, Signals from the lysosome: a control centre for cellular clearance and energy metabolism, Nat. Rev. Mol. Cell Biol. 14 (2013) 283–296, https://doi.org/10.1038/nrm3565.
[50] N. Mizushima, T. Yoshimori, How to interpret LC3 immunoblotting, Autophagy 3 (2007) 542–545.
[51] Y. Kabeya, N. Mizushima, T. Ueno, A. Yamamoto, T. Kirisako, T. Noda, E. Kominami, Y. Ohsumi, T. Yoshimori, LC3, a mammalian homologue of yeast Apg8p, is localized in autophagosome membranes after processing, EMBO J. 19 (2000) 5720–5728, https://doi.org/10.1093/emboj/19.21.5720.
[52] I. Tanida, N. Minematsu-Ikeguchi, T. Ueno, E. Kominami, Lysosomal turnover, but not a cellular level, of endogenous LC3 is a marker for autophagy, Autophagy 1 (2005) 84–91, https://doi.org/10.4161/auto.1.2.1697.
[53] G. Bjørkøy, T. Lamark, S. Pankiv, A. Øvervatn, A. Brech, T. Johansen, Monitoring autophagic degradation of p62/SQSTM1, Methods Enzymol., Elsevier, Inc., 2009, pp. 181–197, https://doi.org/10.1016/S0076-6879(08)03612-4.
[54] L. Calzolai, F. Franchini, D. Gilliland, F. Rossi, Protein–nanoparticle interaction: identification of the ubiquitin–gold nanoparticle interaction site, Nano Lett. 10 (2010) 3101–3105, https://doi.org/10.1021/nl101746v.
[55] K.K. Liu, W.R. Qiu, E. Naveen Raj, H.F. Liu, H.S. Huang, Y.W. Lin, C.J. Chang, T.H. Chen, C. Chen, H.C. Chang, J.K. Hwang, J.I. Chao, Ubiquitin-coated nanodiamonds bind to autophagy receptors for entry into the selective autophagy pathway, Autophagy 13 (2017) 187–200, https://doi.org/10.1080/15548627.2016.1254864.
[56] K. Phadwal, J. Alegre-Abarrategui, A.S. Watson, L. Pike, S. Anbalagan, E.M. Hammond, R. Wade-Martins, A. McMichael, P. Klenerman, A.K. Simon, A novel method for autophagy detection in primary cells, Autophagy 8 (2014) 677–689, https://doi.org/10.4161/auto.18935.
[57] R. Rajan, M. Karbowniczek, H.R. Pugsley, M.K. Sabnani, A. Astrinidis, N.M. La-Beck, Quantifying autophagosomes and autolysosomes in cells using imaging flow cytometry, Cytom. Part A 87 (2015) 451–458, https://doi.org/10.1002/cyto.a.22652.
[58] L. Popp, L. Segatori, Differential autophagic responses to nano-sized materials, Curr. Opin. Biotechnol. 36 (2015) 129–136, https://doi.org/10.1016/j.copbio.2015.08.016.
[59] R.M. Perera, S. Stoykova, B.N. Nicolay, K.N. Ross, J. Fitamant, M. Boukhali, J. Lengrand, V. Deshpande, M.K. Selig, C.R. Ferrone, J. Settleman, G. Stephanopoulos, N.J. Dyson, R. Zoncu, S. Ramaswamy, W. Haas, N. Bardeesy, Transcriptional control of autophagy-lysosome function drives pancreatic cancer metabolism, Nature (2015), https://doi.org/10.1038/nature14587.
[60] R. Mathew, E. White, Autophagy in tumorigenesis and energy metabolism: friend by day, foe by night, Curr. Opin. Genet. Dev. 21 (2011) 113–119, https://doi.org/10.1016/J.GDE.2010.12.008.